

Supporting Information for

An inverse opal $\text{Cu}_2\text{Nb}_{34}\text{O}_{87}$ anode for high-performance Li^+ storage

Xiangzhen Zhu^{a,b}, Guisheng Liang^b, Qingfeng Fu^b, Renjie Li^b, Yongjun Chen^{b,*},

Yicheng Bi^c, Duo Pan^{d,f}, Rajib Das^e, Chunfu Lin^{a,*}, Zhanhu Guo^{c,*}

Experimental section

Material preparation

Monodispersed polystyrene (PS) sphere dispersion was synthesized by using a soap-free emulsion polymerization method [S1]. Then, the PS spheres were close-packed into colloidal crystals by centrifugation (3000 rpm, 12 h), and dried at 60 °C for 12 h.

The metal precursor solution was obtained by dissolving a desired amount of mixed metal salt (Cu:Nb=1:17, molar ratio) into absolute ethanol. Typically, 0.5 mmol copper nitrate hydrate ($\text{Cu}(\text{NO}_3)_2 \cdot x\text{H}_2\text{O}$, 99.99%, Macklin) and 8.5 mmol niobium ethoxide ($\text{Nb}(\text{OC}_2\text{H}_5)_5$, 99.999%, Sigma–Aldrich) were dissolved into 9 mL absolute ethanol (99.5%, Macklin) under vigorous stirring to form a transparent solution with a light blue colour. Then, 1.5 g PS colloidal crystals were soaked in the

above metal precursor solution for 3 h. Due to capillarity, a certain amount of the solution was impregnated to the macropores in the PS template. The excess solution was removed from the impregnated PS template by filtration. The obtained powder was dried at 60 °C for 12 h in air, and calcined in a tube furnace under an air flow to remove the template and to crystallize $\text{Cu}_2\text{Nb}_{34}\text{O}_{87}$. The calcination temperature was raised to 850 °C at a rate of 1 °C min^{-1} , and 850 °C was kept for 4 h.

Material characterization

A powder X-ray diffraction (XRD) measurement was performed on a Bruker D8 Advance diffractometer to study the crystal structure. The chemical valences of the cations were determined by using an X-ray photoelectron spectrometer (XPS, Thermo Escalab 250Xi, USA). The particle size, morphology and microstructure were systematically investigated by using a field-emission scanning electron microscope (FESEM, Hitachi S-4800, Japan) and high-resolution transmission electron microscope (HRTEM, FEI Tecnai G2 F20 STWIN, USA). A N_2 adsorption/desorption isotherm for calculating the Branauer–Emmett–Teller (BET) specific surface area was recorded by using a surface area analyzer (ASAP 2020, USA).

Electrochemical test

To examine the electrochemical properties of IO- $\text{Cu}_2\text{Nb}_{34}\text{O}_{87}$, a CR2016-type IO- $\text{Cu}_2\text{Nb}_{34}\text{O}_{87}$ /Li half cell and a LiMn_2O_4 //IO- $\text{Cu}_2\text{Nb}_{34}\text{O}_{87}$ full cell were assembled in an glove box filling with pure Ar. The working electrodes were prepared by coating a

uniform mixture of 65 wt% active materials (IO-Cu₂Nb₃₄O₈₇ or LiMn₂O₄ (RDF15B, Shenzhen Kejingstar Technologies Ltd.)), 10 wt% polyvinylidene fluoride (PVDF) and 25 wt% conductive carbon (Super P[®]) on Cu-plate (for IO-Cu₂Nb₃₄O₈₇) or Al-plate (for LiMn₂O₄) current collectors. The mass loading of IO-Cu₂Nb₃₄O₈₇ in the composite electrodes was ~1.0 mg cm⁻², and that of LiMn₂O₄ was ~3.0 mg cm⁻². The N/P ratio in the full cell was ~1:1.1. 1 M LiPF₆ dissolved in 1:1:1 (vol/vol/vol) ethylene carbonated (EC)/dimethyl carbonate (DMC)/diethylene carbonate (DEC) served as electrolyte. Celgard[®] 2325 microporous polypropylene films were employed as separators. A Li foil was used as the counter electrode in the IO-Cu₂Nb₃₄O₈₇/Li half cell. The galvanostatic discharge/charge tests were conducted on an automatic battery testing system (CT-3008, Neware, China) at 25 °C. The cyclic voltammetry (CV) curves were recorded on an electrochemical workstation (CHI660E, Chenhua, China) at 25 °C.

Calculation of apparent Li⁺ diffusion coefficients

The apparent Li⁺ diffusion coefficients (*D*) of IO-Cu₂Nb₃₄O₈₇ were calculated from CV data (Fig. 3f) based on the classical Randles-Sevcik equation (Fig. 3g):

$$I_p = 2.69 \times 10^5 \times n^{1.5} C S D^{0.5} \nu^{0.5} \quad (S1)$$

where *I_p*, *n*, *C*, *S*, and *ν* are the peak current of the intensive cathodic/anodic peak, the charge transfer number (1), the allowed Li⁺ molar concentration in the Cu₂Nb₃₄O₈₇ crystals (32.185 mol L⁻¹), the electrode area of IO-Cu₂Nb₃₄O₈₇ (1 cm²), and the scanning rate, respectively. The calculations show that IO-Cu₂Nb₃₄O₈₇ owns large

apparent Li^+ diffusion coefficients of $5.2 \times 10^{-11} \text{ cm}^2 \text{ s}^{-1}$ for lithiation and $6.8 \times 10^{-11} \text{ cm}^2 \text{ s}^{-1}$ for delithiation.

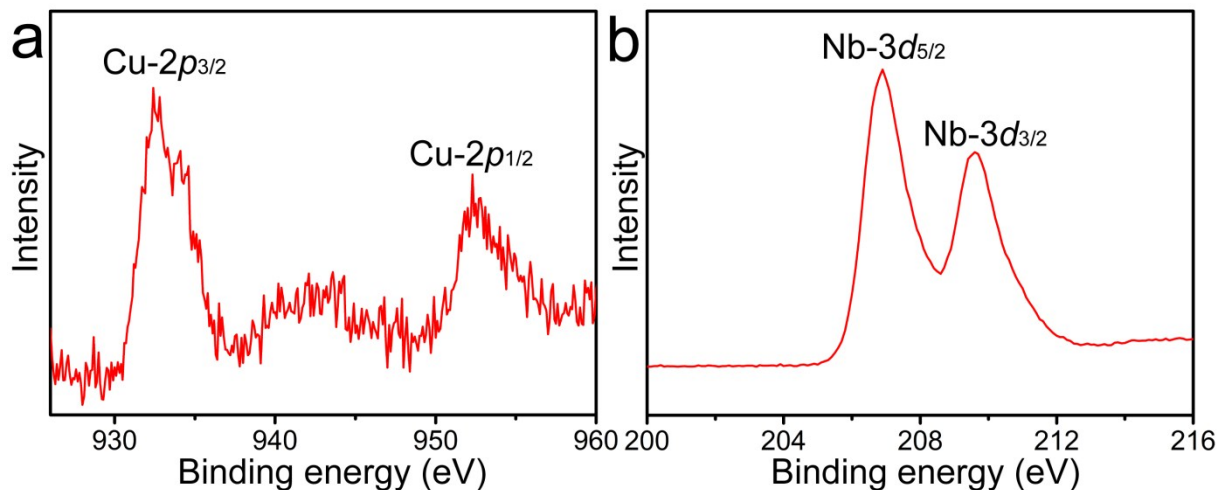


Fig. S1. XPS spectra of IO-Cu₂Nb₃₄O₈₇: (a) Cu-2p and (b) Nb-3d.

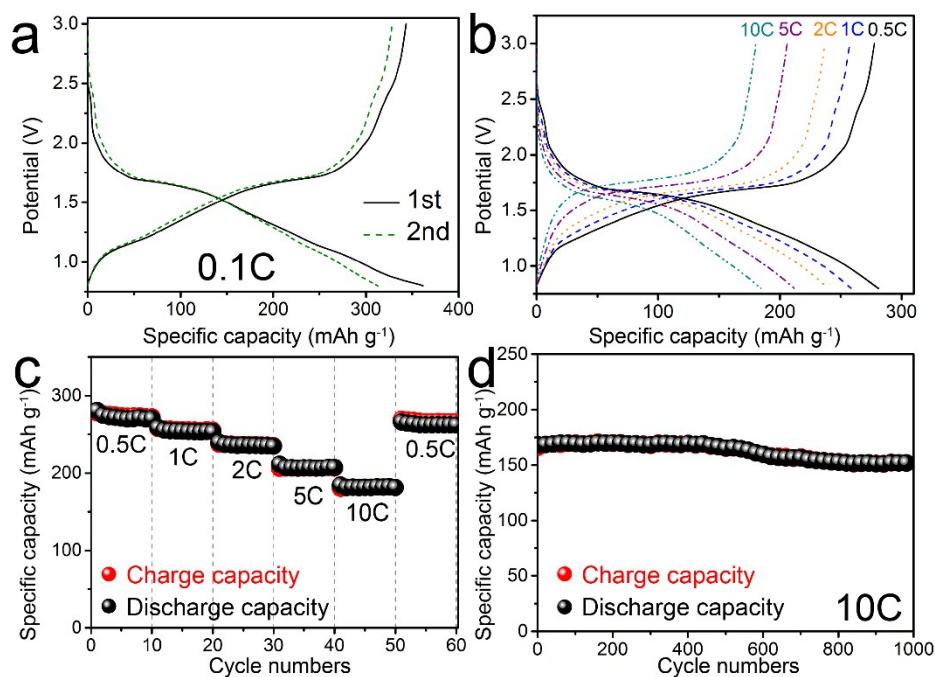


Fig. S2. Electrochemical characterizations of Cu₂Nb₃₄O₈₇ micron-sized particles: (a) discharge/charge profiles at 0.1C, (b) discharge/charge profiles at different C-rates, (c) rate performance, and (d) cycling stability at 10C.

Table S1. Comparisons of electrochemical performance of IO-Cu₂Nb₃₄O₈₇ with typical niobium-based oxide anode materials previously reported.

Material	Current rate	Capacity after cycling (mAh g ⁻¹)	Reference
IO-Cu ₂ Nb ₃₄ O ₈₇	10C	~166 at 1000 th cycles	This work
Cu ₂ Nb ₃₄ O ₈₇ micron-sized particles	10C	~151 at 1000 th cycles	[S2]
Three-dimensionally ordered macroporous T-Nb ₂ O ₅	10C	~124 at 100 th cycles	[S3]
TiNb ₂ O ₇ nanoparticles	10C	~123 at 500 th cycles	[S4]
TiNb ₂ O ₇ nanofibers	5C	~170 at 500 th cycles	[S5]
TiNb ₂ O ₇ nanorods	10C	~140 at 100 th cycles	[S6]
Three-dimensionally ordered macroporous TiNb ₂ O ₇	10C	~87 at 100 th cycles	[S7]
Ti ₂ Nb ₁₀ O ₂₉ hollow nanofibers	10C	~123 at 500 th cycles	[S8]
Porous Ti ₂ Nb ₁₀ O ₂₉ nanospheres	10C	~141 at 1000 th cycles	[S9]
WNb ₁₂ O ₃₃ nanowires	3C	~140 at 700 th cycles	[S10]
GeNb ₁₈ O ₄₇ nanofibers	2C	~162 at 200 th cycles	[S11]
VNb ₉ O ₂₅ nanoribbons	3C	~132 at 500 th cycles	[S12]
W ₉ Nb ₈ O ₄₇ nanofibers	5C	~113 at 1000 th cycles	[S13]
GaNb ₁₁ O ₂₉ nanowebs	10C	~153 at 1000 th cycles	[S14]

References

- [S1] L. Fu, T. Zhang, Q. Cao, H. Zhang, Y. Wu, Preparation and characterization of three-dimensionally ordered mesoporous titania microparticles as anode material for lithium ion battery, *Electrochem. Commun.* 9 (2007) 2140–2144.
- [S2] L.T. Yang, X.Z. Zhu, X.H. Li, X.B. Zhao, K. Pei, W.B. You, X. Li, Y.J. Chen, C.F. Lin, R.C. Che, Conductive copper niobate: superior Li⁺-storage capability and novel Li⁺-transport mechanism, *Adv. Energy Mater.* 9 (2019) 1902174.
- [S3] S.F. Lou, X.Q. Cheng, L. Wang, J.L. Gao, Q. Li, Y.L. Ma, Y.Z. Gao, P.J. Zuo, C.Y. Du, G.P. Yin, High-rate capability of three-dimensionally ordered microporous T-Nb₂O₅ through Li⁺ intercalation pseudocapacitance, *J. Power Sources*, 361 (2017) 80–86.
- [S4] S.F. Lou, Y.L. Ma, X.Q. Cheng, J.L. Gao, Y.Z. Gao, P.J. Zuo, C.Y. Du, G.P. Yin, Facile synthesis of nanostructured TiNb₂O₇ anode materials with superior performance for high-rate lithium ion batteries, *Chem. Commun.* 51 (2015) 17293–17296.
- [S5] H. Park, T. Song, U. Paik, Porous TiNb₂O₇ nanofibers decorated with conductive Ti_{1-x}Nb_xN bumps as a high power anode material for Li-ion batteries, *J. Mater. Chem. A* 3 (2015) 8590–8596.
- [S6] L. Hu, C.F. Lin, C.H. Wang, C. Yang, J.B. Li, Y.J. Chen, S.W. Lin, TiNb₂O₇ nanorods as a novel anode materials for secondary lithium-ion batteries. *Funct. Mater. Lett.* 9 (2016) 1642004.
- [S7] S.F. Lou, X.Q. Cheng, Y. Zhao, A. Lushington, J.L. Gao, Q. Li, P.J. Zuo, B.Q. Wang, Y.Z. Gao, Y.L. Ma, C.Y. Du, G.P. Yin, X.L. Sun, Superior performance of

ordered macroporous TiNb_2O_7 anodes for lithium ion batteries: understanding from the structural and pseudocapacitive insights on achieving high rate capability, *Nano Energy* 34 (2017) 15–25.

[S8] Q.F. Fu, J.R. Hou, R.H. Lu, C.F. Lin, Y. Ma, J.B. Li, Y.J. Chen, Electrospun $\text{Ti}_2\text{Nb}_{10}\text{O}_{29}$ hollow nanofibers as high-performance anode materials for lithium-ion batteries, *Mater. Lett.* 214 (2018) 60–63.

[S9] S.F. Lou, X.Q. Cheng, J.L. Gao, Q. Li, L. Wang, Y. Cao, Y.L. Ma, P.J. Zuo, Y.Z. Gao, C.Y. Du, H. Huo, G.P. Yin, Pseudocapacitive Li^+ intercalation in porous $\text{Ti}_2\text{Nb}_{10}\text{O}_{29}$ nanospheres enables ultra-fast lithium storage, *Energy Storage Mater.* 11 (2018) 57–66.

[S10] L. Yan, H. Lan, H.X. Yu, S.S. Qian, X. Cheng, N.B. Long, R.F. Zhang, M. Shui, J. Shu, Electrospun $\text{WNb}_{12}\text{O}_{33}$ nanowires: superior lithium storage capability and their working mechanism, *J. Mater. Chem. A* 5 (2017) 8972–8980.

[S11] F.M. Ran, X. Cheng, H.X. Yu, R.T. Zheng, T.T. Liu, X.F. Li, N. Ren, M. Shui, J. Shu, Nano-structured $\text{GeNb}_{18}\text{O}_{47}$ as novel anode host with superior lithium storage performance, *Electrochim. Acta* 282 (2017) 634–641.

[S12] S.S. Qian, H.X. Yu, L. Yan, H.J. Zhu, X. Cheng, Y. Xie, N.B. Long, M. Shui, J. Shu, High-rate long-life pored nanoribbon $\text{VNb}_9\text{O}_{25}$ built by interconnected ultrafine nanoparticles as anode for lithium-ion batteries, *ACS Appl Mater. Interfaces* 9 (2017) 30608–30616.

[S13] L. Yan, X. Cheng, H.X. Yu, H.J. Zhu, T.T. Liu, R.T. Zheng, R.F. Zhang, M. Shui, J. Shu, Ultrathin $W_9Nb_8O_{47}$ nanofibers modified with thermal NH_3 for superior electrochemical energy storage, *Energy Storage Mater.* 14 (2018) 159–168.

[S14] X.M. Lou, Q.F. Fu, J. Xu, X. Liu, C.F. Lin, J.X. Han, Y.P. Luo, Y.J. Chen, X.Y. Fan, J.B. Li, $GaNb_{11}O_{29}$ nanowebs as high-performance anode materials for lithium-ion batteries, *ACS Appl. Nano Mater.* 1 (2018) 183–190.